Electrocatalysis

Deutsche Ausgabe: DOI: 10.1002/ange.201510460
Internationale Ausgabe: DOI: 10.1002/anie.201510460

Ultrathin Free-Standing Ternary-Alloy Nanosheets

*Jong Wook Hong, Yena Kim, Dae Han Wi, Seunghoon Lee, Su-Un Lee, Young Wook Lee, Sang-Il Choi, and Sang Woo Han**

Abstract: *A synthesis strategy for the preparation of ultrathin free-standing ternary-alloy nanosheets is reported. Ultrathin Pd-Pt-Ag nanosheets with a thickness of approximately 3 nm were successfully prepared by co-reduction of the metal precursors in an appropriate molar ratio in the presence of CO. Both the presence of CO and the interplay between the constituent metals provide fine control over the anisotropic two-dimensional growth of the ternary-alloy nanostructure. The prepared Pd-Pt-Ag nanosheets were superior catalysts of ethanol electrooxidation owing to their specific structural and compositional characteristics. This approach will pave the way for the design of multicomponent 2D nanomaterials with unprecedented functions.*

Noble-metal nanocrystals (NCs) with controlled shapes and morphologies are still receiving great attention owing to their fascinating catalytic properties in a wide range of reactions.[1] Among the various shapes that noble-metal NCs can adopt, ultrathin 2D sheet-like structures with single- or few-atomic-layer thickness (< 5 nm) have recently been of particular interest. Their relatively high surface energy, which is a result of their high surface to volume ratio, and the high density of unsaturated atoms endow them with excellent catalytic activities.[2] For instance, the electrocatalytic activity of ultrathin Pd nanosheets in formic acid oxidation is 2.5 times higher than that of a commercial Pd catalyst,[3] and ultrathin Rh nanosheets showed enhanced catalytic performance in hydrogenation and hydroformylation reactions compared to spherical Rh nanoparticles and a commercial Rh/C catalyst.[4]

The incorporation of other metals into noble-metal NCs to prepare multimetallic alloy nanostructures has been intensively explored to promote and optimize their catalytic activity, selectivity, and stability for various reactions.[5] For example, in the case of the electrooxidation of alcohols, such as methanol and ethanol, alloying Pt or Pd with oxophilic metals, such as Ru, Rh, Ni, Sn, or Ag, can facilitate the formation of surface-bound OH (OH_{ads}) species, which can drive the oxidation of alcohols without the production of poisoning by-products, such as CO.[6] Strasser et al. also demonstrated that a Pt-Rh-Ni ternary-alloy nanocatalyst exhibited enhanced ethanol oxidation reaction (EOR) activity owing to the synergistic effects of C–C bond cleavage on Rh and OH adsorption on active $Ni(OH)_x$.[7] In this regard, the availability of a synthesis method to produce multimetallic alloy NCs with an ultrathin sheet-like structure is highly desirable for developing novel catalysts with superior catalytic performance.

As noble metals are non-layer-structured materials, both 2D anisotropic growth and stabilization of unsaturated atoms on lateral planes should be considered to realize ultrathin 2D noble-metal nanostructures.[2] Furthermore, careful consideration of the different inherent growth habits of all constituent metals is required for the synthesis of ultrathin multimetallic alloy nanostructures. Accordingly, the synthesis of ultrathin alloy nanosheets remains a great challenge. In fact, the preparation of ultrathin multimetallic alloy nanosheets has rarely been reported,[8] although a few examples of bimetallic core–shell nanosheets have been described.[9] To the best of our knowledge, the synthesis of ultrathin trimetallic alloy nanosheets has not been achieved thus far.

Herein, we demonstrate the facile aqueous synthesis of ultrathin free-standing trimetallic alloy nanosheets for the first time. By the co-reduction of Pd, Pt, and Ag precursors with ascorbic acid (AA) in the presence of cetyltrimethylammonium chloride (CTAC) and CO, ultrathin Pd-Pt-Ag ternary-alloy nanosheets with a thickness of approximately 3 nm were successfully prepared. During the formation of the nanosheets, CO plays a pivotal role in stabilizing the basal planes of growing nanosheets, thus facilitating the anisotropic 2D growth. Furthermore, the interplay between three constituent metals, namely Pd, Pt, and Ag, during the synthesis is critical to form the ternary-alloy Pd-Pt-Ag nanosheets. Notably, the prepared Pd-Pt-Ag alloy nanosheets showed greatly improved electrocatalytic activity towards the EOR compared to their nanoparticle counterparts and commercial Pd/C and Pt/C catalysts owing to their specific structural and compositional characteristics.

In a typical synthesis of Pd-Pt-Ag alloy nanosheets, aqueous solutions of K_2PdCl_4, K_2PtCl_4, $AgNO_3$ (molar ratio of $K_2PdCl_4/K_2PtCl_4/AgNO_3 = 1:1:1$), and AA were sequentially injected into a CO-saturated aqueous solution of CTAC, and the resultant mixture was heated at 95 °C for two hours (for experimental details, see the Supporting Information). A typical transmission electron microscopy (TEM) image of the product is shown in Figure 1a, indicating the successful formation of nanosheets (ca. 95% yield) with an average lateral length of 69 ± 11 nm. A high-magnification TEM image shows a weak contrast between nanosheet and background, demonstrating the ultrathin nature of the nanosheet

[*] Dr. J. W. Hong, Y. Kim, D. H. Wi, S. Lee, S.-U. Lee, Y. W. Lee, Prof. S. W. Han
Center for Nanotectonics
Department of Chemistry and KI for the NanoCentury, KAIST
Daejeon 34141 (Korea)
E-mail: sangwoohan@kaist.ac.kr
Prof. S.-I. Choi
Department of Chemistry and Green-Nano Materials Research Center, Kyungpook National University
Daegu 41566 (Korea)

Supporting information and ORCID(s) from the author(s) for this article are available on the WWW under http://dx.doi.org/10.1002/anie.201510460.

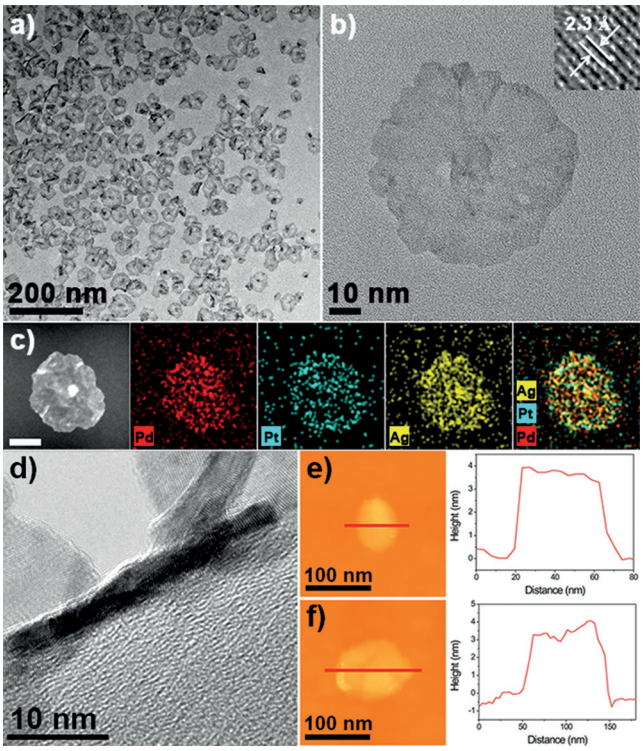

Figure 1. a) Low- and b) high-magnification TEM images of the Pd-Pt-Ag nanosheets (the inset shows the visible lattice fringes). c) HAADF-STEM image and corresponding EDS elemental maps of a Pd-Pt-Ag nanosheet. Scale bar: 20 nm. d) HRTEM image of the side face of a Pd-Pt-Ag nanosheet. e, f) AFM images and corresponding height profiles of Pd-Pt-Ag nanosheets supported on a Si wafer.

(Figure 1 b). The compositional structure of a nanosheet was investigated by high-angle annular dark-field–scanning TEM–energy-dispersive X-ray spectroscopy (HAADF-STEM-EDS), which clearly confirmed the Pd-Pt-Ag ternary-alloy structure (Figure 1 c). The Pd/Pt/Ag atomic ratios of the prepared nanosheets determined by EDS elemental analysis and inductively coupled plasma mass spectrometry (ICP-MS) were 43:28:29 and 41:32:27, respectively. The X-ray diffraction (XRD) pattern of the Pd-Pt-Ag nanosheets showed that all of the diffraction peaks appeared between the known corresponding peaks of pure face-centered cubic Pd, Pt, and Ag, revealing the phase purity of the nanosheets (Supporting Information, Figure S1). The *d* spacing of adjacent lattice fringes of the Pd-Pt-Ag nanosheet was 2.3 Å (inset of Figure 1 b), which matches well with the calculated value of the (111) planes of a Pd-Pt-Ag alloy with the same composition (2.28 Å based on Vegard's law).[10] A high-magnification high-resolution TEM (HRTEM) image, the corresponding fast Fourier transform pattern (Figure S2), and the XRD pattern of nanosheets preferentially oriented parallel to the supporting substrate (Figure S3) further confirmed that the basal plane of the nanosheets is the {111} facet. X-ray photoelectron spectroscopy (XPS) measurements of the Pd-Pt-Ag nanosheets revealed that Pd, Pt, and Ag are in the metallic state (Figure S4).

To evaluate the thickness of the Pd-Pt-Ag nanosheets, we obtained HRTEM images that show the side faces of the Pd-Pt-Ag nanosheets by using a lacey carbon grid. As shown in Figure 1 d, the thickness of the nanosheets was approximately 3 nm, which corresponds to about 15 atomic layers. The thickness of the Pd-Pt-Ag nanosheets was further confirmed by recording atomic force microscopy (AFM) images and height profiles of Pd-Pt-Ag nanosheets supported on a Si wafer (Figure 1 e, f). The AFM height profiles revealed the thickness of the nanosheets to be about 4 nm, which is larger than that measured by TEM. This is likely due to the presence of residual surfactant molecules on the nanosheets.[3]

To investigate the shape evolution of the Pd-Pt-Ag nanostructures over the course of the reaction, samples collected at different reaction times were analyzed by TEM (Figure S5). At the initial stage of the reaction (reaction time = 5 min), small nanoparticles (1.5–3 nm) were present (Figure S5 a). When the reaction time was increased to 7 min, 5–10 nm 2D sheet-like nanostructures began to appear (Figure S5 b). As the reaction time was further increased, the size of the nanosheets gradually increased (Figure S5 c–e). The nanosheets produced at a reaction time of 30 min were similar in size to the typical Pd-Pt-Ag nanosheets (Figure S5 e). A further increase in reaction time resulted in no discernible changes in the size of the nanosheets (Figure S5 f). Notably, the nanosheets formed at the early stage of reaction also have the Pd-Pt-Ag ternary-alloy structure with compositions similar to that of the final nanosheets (Figure S6).

The introduction of CO gas in the synthesis is essential for the formation of the Pd-Pt-Ag nanosheets. By monitoring the shape of the Pd-Pt-Ag nanostructures formed under various reaction conditions (Figure 2), we found that nanosheet structures were obtained when a sufficient amount of CO was present in the reaction solution. In the absence of CO, dendritic nanoparticles were formed (Figure 2 a), whereas irregularly shaped nanoparticles with several protrusions were produced when the reaction solution was purged with CO gas for 1 min with a flow rate of 150 $cm^3 min^{-1}$ (Figure 2 b). By extending the CO purging time to 3 and 5 min, mixtures of nanosheets and irregularly shaped nanoparticles were produced (Figure 2 c, d, respectively). Noticeably, when the CO purging time was increased to 10 or 20 min, nanosheets were obtained as the major products (Figure 2 e, f, respectively). In this regard, the CO purging time was set to be 20 min in the standard synthesis of the Pd-Pt-Ag nanosheets. On the other hand, TEM images of products prepared in the absence of CTAC under otherwise identical experimental conditions showed that ultrathin Pd-Pt-Ag nanosheets were still obtained without CTAC (Figure S7), further confirming the contribution of CO to the formation of nanosheets. However, agglomeration between nanosheets was observed in the absence of CTAC, implying that this process is prevented by CTAC. These results explicitly demonstrate the important role of CO in the formation of ultrathin free-standing Pd-Pt-Ag nanosheets. In fact, CO molecules can stabilize the basal {111} planes of growing nanosheets by adsorption, thus facilitating anisotropic 2D growth.[11]

Through several control experiments, we also found that the co-reduction of Pd, Pt, and Ag precursors with an appropriate molar ratio of K_2PdCl_4/K_2PtCl_4 is crucial for the

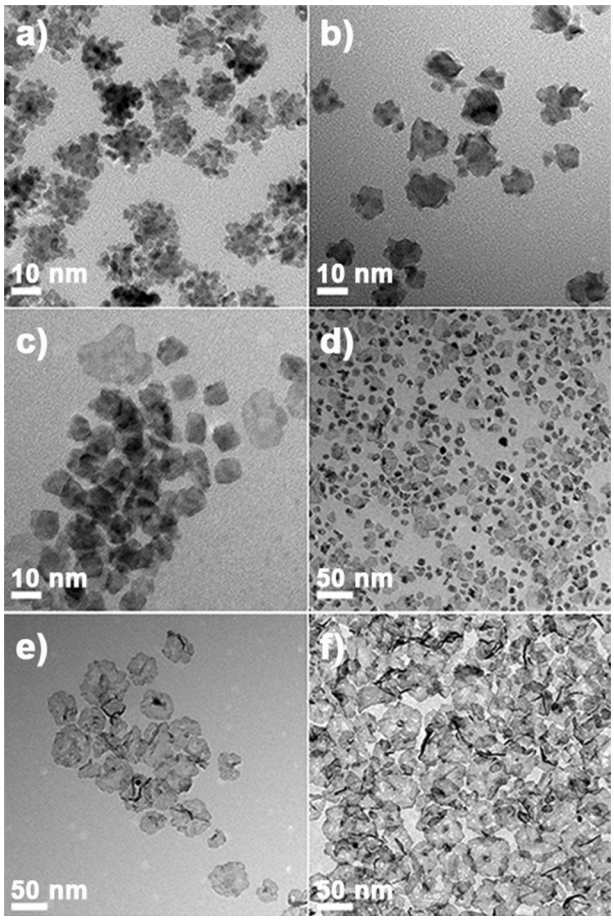

Figure 2. TEM images of nanostructures produced when the reaction solution was purged with CO gas for a) 0, b) 1, c) 3, d) 5, e) 10, and f) 20 min.

generation of Pd-Pt-Ag alloy nanosheets (Figure 3). In the absence of the Pd precursor, dendritic Pt-Ag nanostructures were obtained under synthesis conditions identical to the standard procedure (Figure 3a). The Pd-Pt-Ag nanostructures started to adopt a sheet-like morphology when the K_2PdCl_4/K_2PtCl_4 molar ratio was increased to 0.25, while rough surfaces with small particulate protrusions were still observed (Figure 3b). An increase in the amount of Pd precursor to a K_2PdCl_4/K_2PtCl_4 ratio of 1, which is the ratio used in the standard synthesis, yielded well-defined Pd-Pt-Ag nanosheets (Figure 3c). However, when the molar ratio of K_2PdCl_4/K_2PtCl_4 was further increased to 4, several holes appeared in the nanosheets (Figure 3d), and reactions in the absence of the Pt precursor produced wrinkled nanosheets (Figure 3e). The EDS-determined Pd/Pt/Ag atomic ratios of the products shown in Figure 3 are 0:80:20 (a), 25:51:24 (b), 43:28:29 (c), 59:19:22 (d), and 67:33:0 (e). These results, along with the aforementioned role of CO in stabilizing the basal {111} planes of growing nanosheets, indicate that Pd primarily contributes to the formation of ultrathin nanosheets by interacting with CO. Furthermore, the poor structural integrity of nanosheets synthesized with high percentages of Pd implies that the presence of Pt can impart structural stability to nanosheets, which is in line with previous studies on other multimetallic nanostructures.[12]

On the other hand, we performed the synthesis in the absence of the Ag precursor while keeping the other reaction conditions unchanged to identify the role of the Ag component in the formation of nanosheets. Interestingly, ultrathin sheet-like nanostructures were still generated (Figure S8a,b). However, HAADF-STEM-EDS elemental analysis of the prepared nanosheets showed that the Pd signal was of higher intensity than the Pt signal in the inner region of the nanosheet (Pd/Pt = 89:11), while the edge region of the nanosheet was largely composed of Pt (Pd/Pt = 17:83; Figure S8c–f). This finding indicates that Ag has a great influence on the formation of a uniform Pd-Pt-Ag ternary-alloy structure. The production of non-uniform alloy structures in the absence of Ag is likely due to the different reduction kinetics of the Pd and Pt precursors. Under the experimental conditions employed for the synthesis of Pd-Pt nanosheets, the reduction rate of the Pd precursor is higher than that of the Pt precursor (Figure S9a,c). Therefore, sheet-like seed nanostructures mostly composed of Pd might be formed first, and then the remaining metal precursors are deposited preferentially onto the side faces of the formed nanosheets, which have a higher surface energy than the basal planes, resulting in the formation of the observed Pd-Pt nanosheets. On the contrary, when the Ag precursors co-exist in the reaction medium, the reduction kinetics of the metal precursors are modified owing to multiple mutual interactions, resulting in the modulation of the nucleation and growth habits.[13] In fact, in the presence of the Ag precursor, the

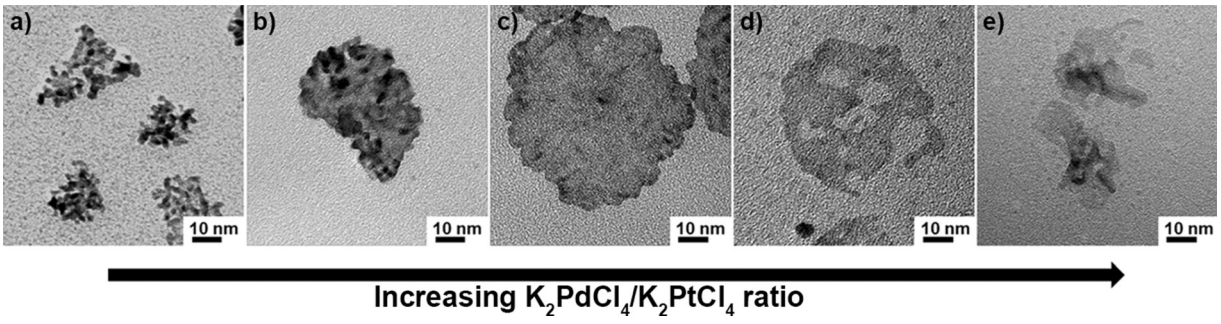

Figure 3. TEM images of nanostructures prepared with different molar ratios of $K_2PdCl_4/K_2PtCl_4/AgNO_3$: a) 0:0.6:0.3, b) 0.12:0.48:0.3, c) 0.3:0.3:0.3, d) 0.48:0.12:0.3, e) 0.6:0:0.3.

reduction of the Pd precursor was slowed down, while that of the Pt precursor was accelerated (Figure S9b,d). The modified reduction kinetics could thus induce the formation of uniform Pd-Pt-Ag ternary-alloy nanosheets under our synthesis conditions.

The catalytic performance of the prepared Pd-Pt-Ag nanosheets was investigated by using the electrocatalytic EOR as a model reaction, and the results were compared with those of Pd-Pt nanosheets (Figure S8), Pd-Pt-Ag nanodendrites (Figure S10a), Pd-Pt nanodendrites (Figure S10b), and commercial Pd/C and Pt/C catalysts. The Pd-Pt-Ag and Pd-Pt nanodendrites were prepared in the absence of CO under experimental conditions that were otherwise identical to those applied in the synthesis of the Pd-Pt-Ag and Pd-Pt nanosheets, respectively. Before electrochemical measurements, glassy carbon electrodes (GCEs) modified with the catalysts were thoroughly washed with solvents and then electrochemically cleaned to remove residual stabilizing agents on the catalyst surfaces (see the Supporting Information for details). The electrochemically active surface areas (ECSAs) of the catalysts calculated from the charge required for oxygen desorption in the cyclic voltammograms (CVs) of the catalysts in 0.1 M KOH (Figure S11) were 54.7, 53.9, 26.8, 28.4, 30.7, and 34.5 $m^2 g^{-1}$ for the Pd-Pt-Ag nanosheets, Pd-Pt nanosheets, Pd-Pt-Ag nanodendrites, Pd-Pt nanodendrites, Pd/C, and Pt/C, respectively. Notably, the ultrathin Pd-Pt-Ag and Pd-Pt nanosheets showed ECSA values that were approximately two times larger than those of their nanodendrite counterparts owing to their 2D ultrathin sheet-like structures. Figure 4a shows the CVs obtained for the EOR with different catalysts, in which the characteristic ethanol oxidation peaks were identified in the forward and backward scans. It is apparent that the EOR activity of the catalysts distinctly depends on their morphology and composition (Figure 4b). The Pd-Pt-Ag and Pd-Pt nanosheets exhibited remarkable improvements in EOR activity compared to the other catalysts. This indicates that the large active surface area associated with the ultrathin 2D nanosheet structure of the Pd-Pt-Ag and Pd-Pt nanosheets can boost their electrocatalytic properties. It is noteworthy that the Pd-Pt-Ag nanosheets showed higher catalytic activity toward the EOR compared to the Pd-Pt nanosheets, signifying the positive synergy of the incorporation of Ag into Pd-Pt nanosheets for the EOR.

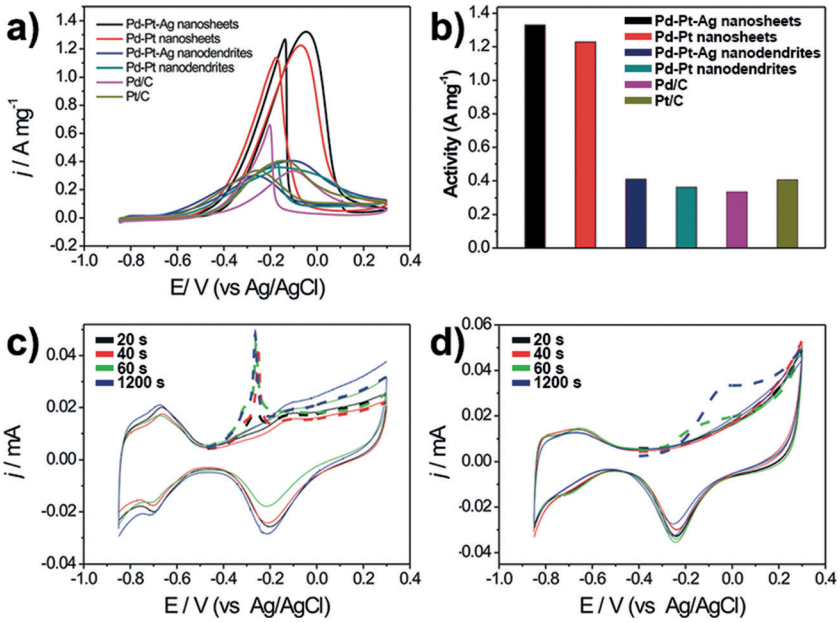

Figure 4. a) CVs obtained with various catalysts in 0.1 M KOH and 0.5 M ethanol at a scan rate of 50 $mV s^{-1}$. b) Catalytic activities of the different materials in the EOR. c,d) CO stripping voltammograms for the Pd-Pt (c) and Pd-Pt-Ag nanosheets (d) in 0.1 M KOH at a scan rate of 50 $mV s^{-1}$. The first and second scans are depicted as dashed and solid lines, respectively. Before the CO stripping tests, the working electrodes were hold at −0.1 V vs. Ag/AgCl during CO purging for the indicated periods of time.

It has been generally accepted that the EOR on metal (M) surfaces in alkaline media proceeds via the reactive-intermediate and/or the poisoning-intermediate (CO) pathway (see Figure S12).[14] In the reactive-intermediate pathway, $M{-}OH_{ads}$ and $M{-}(COCH_3)_{ads}$ intermediates are combined to generate acetate anions. On the other hand, in the poisoning-intermediate pathway, $M{-}(COCH_3)_{ads}$ solely decomposes to $M{-}CO_{ads}$ and $M{-}(CH_3)_{ads}$, which block active sites of the catalyst and thus deteriorate the activity. Accordingly, catalysts with facile OH_{ads} generation and high CO tolerance will have improved catalytic efficacies for the EOR. The higher catalytic activity of the Pd-Pt-Ag nanosheets compared to the Pd-Pt nanosheets might thus be attributed to the enhanced OH_{ads} formation and CO tolerance upon the incorporation of Ag. Indeed, the incorporation of Ag into Pd-Pt can facilitate the formation of OH_{ads} on the nanostructure surface owing to the exposed oxophilic Ag sites[15] and the changes in electronic structure that are due to the formation of the Pd-Pt-Ag alloy,[14d] thus driving the EOR preferentially through the efficient reactive-intermediate pathway. In fact, XPS measurements of the Pd 3d and Pt 4f core levels of the Pd-Pt-Ag and Pd-Pt nanosheets showed that the electronic structures of Pd and Pt were somewhat modified upon the incorporation of Ag (Figure S4a,b). An analogous tendency was also observed in the XPS spectra of the Pd-Pt-Ag and Pd-Pt nanodendrites. On the other hand, CO stripping tests further indicated that the Pd-Pt-Ag nanosheets have a higher CO tolerance than Pd-Pt nanosheets (Figure 4c,d). By holding the catalyst-modified GCEs at −0.1 V vs. Ag/AgCl for different times from 20 to 1200 s during CO purging, the amount of CO_{ads} on the surface of the catalyst could be modulated. In the case of the Pd-Pt nanosheets, the peak associated with the oxidative removal of CO appeared in the CO stripping voltammogram even after 20 s potential holding for CO adsorption (Figure 4c). As the time of potential holding was increased to 60 s, the intensity of the CO stripping peak gradually increased. A further increase in the holding time resulted in no significant changes in the intensity of the

CO stripping peak, indicating that the surface of the Pd-Pt nanosheets was saturated by CO_{ads} in 60 s. On the contrary, in the case of the Pd-Pt-Ag nanosheets, the CO stripping peak started to appear after 60 s potential holding, and its intensity further increased as the holding time was increased to 1200 s (Figure 4d). Furthermore, the intensity of the CO stripping peak was much lower than that of the Pd-Pt nanosheets for the same holding time. These results definitely demonstrate the superior CO tolerance of the Pd-Pt-Ag nanosheets compared to the Pd-Pt nanosheets.

The electrocatalytic stability of the prepared nanosheets was examined by an accelerated durability test, and the result was compared with those of commercial Pt/C and Pd/C catalysts (Figure S13). After 400 EOR cycles, the activity of the Pd-Pt-Ag nanosheets had decreased to 0.92 $A\,mg^{-1}$, but was still higher than those of pristine Pt/C and Pd/C by factors of 2.4 and 2.8, respectively. The activity of the Pt/C and Pd/C catalysts had decreased to 0.26 and 0.23 $A\,mg^{-1}$, respectively, after the test. A TEM image of Pd-Pt-Ag nanosheets after the durability test demonstrates that the deterioration of the activity of the nanosheets can be ascribed to their structural deformation (Figure S14b). The EDS-determined Pd/Pt/Ag atomic ratio of the nanosheets after the durability test was 40:28:32, which is similar to that of the pristine nanosheets, indicating that the selective removal of a certain element had not occurred. On the other hand, extensive aggregation and coalescence of the nanoparticles were observed for the Pt/C and Pd/C catalysts after the durability test (Figure S14d,f), which can cause the catalytic activity to decrease.

In summary, we have developed a facile synthesis method for the preparation of ultrathin free-standing Pd-Pt-Ag trimetallic alloy nanosheets. The synthesis of the Pd-Pt-Ag nanosheets was achieved by the co-reduction of suitable metal precursors in an appropriate molar ratio in the presence of CO. Both CO and the interplay between the constituent metals facilitate the anisotropic 2D growth of the ternary-alloy nanostructure. The prepared Pd-Pt-Ag nanosheets were excellent electrocatalysts of the EOR owing to their ultrathin 2D structure as well as improved OH_{ads} formation and CO tolerance. We envision that the present approach can be extended to the synthesis of other multicomponent 2D nanomaterials with desired functions and will provide a promising way to develop high-performance catalyst systems. Remarkably, and as an example, Pd-Pt-Rh and Pd-Pt-Ag-Rh nanosheets were also successfully prepared by this method (Figure S15).

Acknowledgements

This work was supported by the Basic Science Research Program through the National Research Foundation of Korea (NRF) funded by the Ministry of Science, ICT & Future Planning (2015R1A3A2033469).

Keywords: alloys · nanosheets · palladium · platinum · silver

How to cite: *Angew. Chem. Int. Ed.* **2016**, *55*, 2753–2758
Angew. Chem. **2016**, *128*, 2803–2808

[1] a) L. Zhang, L. T. Roling, X. Wang, M. Vara, M. Chi, J. Liu, S.-I. Choi, J. Park, J. A. Herron, Z. Xie, M. Mavrikakis, Y. Xia, *Science* **2015**, *349*, 412; b) T. Fujita, P. Guan, K. McKenna, X. Lang, A. Hirata, L. Zhang, T. Tokunaga, S. Arai, Y. Yamamoto, N. Tanaka, Y. Ishikawa, N. Asao, Y. Yamamoto, J. Erlebacher, M. Chen, *Nat. Mater.* **2012**, *11*, 775; c) C. Chen, Y. Kang, Z. Huo, Z. Zhu, W. Huang, H. L. Xin, J. D. Snyder, D. Li, J. A. Herron, M. Mavrikakis, M. Chi, K. L. More, Y. Li, N. M. Markovic, G. A. Somorjai, P. Yang, V. R. Stamenkovic, *Science* **2014**, *343*, 1339; d) J. Gu, Y.-W. Zhang, F. Tao, *Chem. Soc. Rev.* **2012**, *41*, 8050.

[2] a) T. Ling, J.-J. Wang, H. Zhang, S.-T. Song, Y.-Z. Zhou, J. Zhao, X.-W. Du, *Adv. Mater.* **2015**, *27*, 5396; b) C. Tan, H. Zhang, *Nat. Commun.* **2015**, *6*, 7873.

[3] X. Huang, S. Tang, X. Mu, Y. Dai, G. Chen, Z. Zhou, F. Ruan, Z. Yang, N. Zheng, *Nat. Nanotechnol.* **2011**, *6*, 28.

[4] H. Duan, N. Yan, R. Yu, C.-R. Chang, G. Zhou, H.-S. Hu, H. Rong, Z. Niu, J. Mao, H. Asakura, T. Tanaka, P. J. Dyson, J. Li, Y. Li, *Nat. Commun.* **2015**, *5*, 3093.

[5] a) J. W. Hong, D. Kim, Y. W. Lee, M. Kim, S. W. Kang, S. W. Han, *Angew. Chem. Int. Ed.* **2011**, *50*, 8876; *Angew. Chem.* **2011**, *123*, 9038; b) H.-l. Liu, F. Nosheen, X. Wang, *Chem. Soc. Rev.* **2015**, *44*, 3056; c) K. Eid, V. Malgras, P. He, K. Wang, A. Aldalbahi, S. M. Alshehri, Y. Yamauchi, L. Wang, *RSC Adv.* **2015**, *5*, 31147.

[6] a) Y. Wang, G. Wang, G. Li, B. Huang, J. Pan, Q. Liu, J. Han, L. Xiao, J. Lu, L. Zhuang, *Energy Environ. Sci.* **2015**, *8*, 177; b) W. Zhu, J. Ke, S.-B. Wang, J. Ren, H.-H. Wang, Z.-Y. Zhou, R. Si, Y.-W. Zhang, C.-H. Yan, *ACS Catal.* **2015**, *5*, 1995; c) R. Li, Z. Wei, T. Huang, A. Yu, *Electrochim. Acta* **2011**, *56*, 6860; d) S. Beyhan, J.-M. Léger, F. Kadırgan, *Appl. Catal. B* **2014**, *144*, 66; e) Q. Shi, P. Zhang, Y. Li, H. Xia, D. Wang, X. Tao, *Chem. Sci.* **2015**, *6*, 4350.

[7] N. Erini, S. Rudi, V. Beermann, P. Krause, R. Yang, Y. Huang, P. Strasser, *ChemElectroChem* **2015**, *2*, 903.

[8] a) F. Saleem, Z. Zhang, B. Xu, X. Xu, P. He, X. Wang, *J. Am. Chem. Soc.* **2013**, *135*, 18304; b) F. Saleem, B. Xu, B. Ni, H. Liu, F. Nosheen, H. Li, X. Wang, *Adv. Mater.* **2015**, *27*, 2013.

[9] a) X. Huang, S. Tang, B. Liu, B. Ren, N. Zheng, *Adv. Mater.* **2011**, *23*, 3420; b) M. Chen, S. Tang, Z. Guo, X. Wang, S. Mo, X. Huang, G. Liu, N. Zheng, *Adv. Mater.* **2014**, *26*, 8210; c) Z. Fan, X. Huang, Y. Han, M. Bosman, Q. Wang, Y. Zhu, Q. Liu, B. Li, Z. Zeng, J. Wu, W. Shi, S. Li, C. L. Gan, H. Zhang, *Nat. Commun.* **2015**, *6*, 6571; d) Z. Fan, Y. Zhu, X. Huang, Y. Han, Q. Wang, Q. Liu, Y. Huang, C. L. Gan, H. Zhang, *Angew. Chem. Int. Ed.* **2015**, *54*, 5672; *Angew. Chem.* **2015**, *127*, 5764.

[10] a) J. W. Hong, S. W. Kang, B.-S. Choi, D. Kim, S. B. Lee, S. W. Han, *ACS Nano* **2012**, *6*, 2410; b) J. Zeng, Y. Zheng, M. Rycenga, J. Tao, Z.-Y. Li, Q. Zhang, Y. Zhu, Y. Xia, *J. Am. Chem. Soc.* **2010**, *132*, 8552.

[11] a) C. Hu, K. Lin, X. Wang, S. Liu, J. Yi, Y. Tian, B. Wu, G. Chen, H. Yang, Y. Dai, H. Li, N. Zheng, *J. Am. Chem. Soc.* **2014**, *136*, 12856; b) X. Huang, S. Tang, J. Yang, Y. Tan, N. Zheng, *J. Am. Chem. Soc.* **2011**, *133*, 15946.

[12] a) D. Wang, H. L. Xin, Y. Yu, H. Wang, E. Rus, D. A. Muller, H. D. Abruña, *J. Am. Chem. Soc.* **2010**, *132*, 17664; b) K. Eid, H. Wang, V. Malgras, Z. A. Alothman, Y. Yamauchi, L. Wang, *J. Phys. Chem. C* **2015**, *119*, 19947.

[13] a) S. W. Kang, Y. W. Lee, Y. Park, B.-S. Choi, J. W. Hong, K.-H. Park, S. W. Han, *ACS Nano* **2013**, *7*, 7945; b) D. Wang, Y. Li, *Adv. Mater.* **2011**, *23*, 1044; c) R. Ferrando, J. Jellinek, R. L. Johnston, *Chem. Rev.* **2008**, *108*, 845; d) A. R. Tao, S. Habas, P. Yang, *Small* **2008**, *4*, 310; e) R. M. Arán-Ais, F. Dionigi, T. Merzdorf, M. Gocyla, M. Heggen, R. E. Dunin-Borkowski, M. Gliech, J. Solla-Gullón, E. Herrero, J. M. Feliu, P. Strasser, *Nano Lett.* **2015**, *15*, 7473.

[14] a) C. Bianchini, V. Bambagioni, J. Filippi, A. Marchionni, F. Vizza, P. Bert, A. Tampucci, *Electrochem. Commun.* **2009**, *11*, 1077; b) C. Bianchini, P. K. Shen, *Chem. Rev.* **2009**, *109*, 4183; c) P. A. Christensen, S. W. M. Jones, A. Hamnett, *Phys. Chem. Chem. Phys.* **2013**, *15*, 17268; d) S. T. Nguyen, H. M. Law, H. T. Nguyen, N. Kristian, S. Wanga, S. H. Chan, X. Wang, *Appl. Catal. B* **2009**, *91*, 507.

[15] Y. Lu, W. Chen, *ACS Catal.* **2012**, *2*, 84.

Received: November 11, 2015
Revised: December 13, 2015
Published online: January 22, 2016

